Using a Gaussian Process To Optimise Simulation Parameters For Experimental Shock Velocity Results

(Ben Gosling - U1706745)

Simulating ICF experiments accurately is crucial to increasing our ability to predict how future experiments will perform. Hydrodynamic simulation models of ICF implosions use several parameters that control essential physics being modelled, such as laser deposition, laser energy loss, and thermal transport. This paper uses Gaussian process regression techniques to create surrogate models that estimate the optimal value of input parameters to match Freyja simulation results to the experimental shock velocity results found in Goncharov et al. [1]. A Gaussian log-likelihood metric is used to train the surrogate model to compare the simulation and experimental results. The input parameters chosen were those that control aspects of laser deposition, loss and thermal transport, such as electron and ion flux limiter, resonant absorption fraction, LPI loss fraction, and laser energy coupling factor. The created surrogate models match the experimental results well and accurately predict parameters that match the shock coalescence timings and breakout times. However, it was found that this was not always the case, suggesting that improvements to the training procedure should be made in order to get the surrogate to match the shock and breakout timings more frequently.

I. INTRODUCTION

Capsule and laser profile designs in inertial confinement fusion (ICF) are tailored to help maintain the central fuel entropy and limit the growth of hydrodynamic instabilities. By keeping the primary fuel in a degenerate state (i.e. $T < T_{Fermi}$), the fuel can be more readily compressed during the deceleration phase of implosion (Fig. 1).

In general, controlling the central fuel entropy is done by tuning the timings of the laser pulses and capsule dimensions to allow for shocks to coalesce within the main fuel layer to mitigate any increase in shell entropy. The triple-picket ignition design for the national ignition facility (NIF) is an example of how a laser is tuned in intensity and in time in direct drive experiments [2]. Such designs begin with two or three lower power pickets, limiting the strength of the initial shock launched into the target to prevent a significant increase in entropy. The Rankine-Hugonoit relations state that the maximal increase in fuel density by an initial shock can only be by a factor of ≈ 4; however, using the series of timed multiple shocks created by the multiple picket design, this can be increased. Subsequent shocks will only marginally increase entropy as $\Delta s \propto \rho^{-5/3}$, where Δs is the increase in entropy and ρ is the pre-shock density. Thus, as the density increases due to multiple shock compressions, the entropy jump gets smaller and tends towards adiabatic compression.

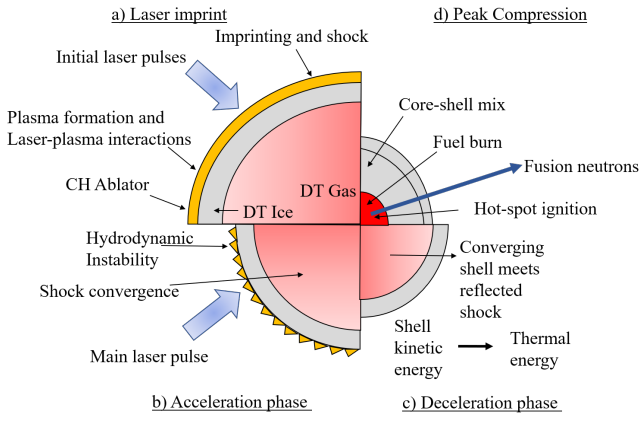

FIG. 1: Simple schematic of the capsule implosion process for direct-drive.

ICF experiments are costly to run and therefore require simulations to be performed to try and accurately predict how a particular target design will behave and use them to help best inform the setup of experiments. Given that a lot of the success of ICF experiments is dependent on how shocks operate within the capsule, it becomes essential to try and accurately produce simulations that model the behaviour observed in experiments. Hydrodynamic models are typically used to simulate ICF implosions, in which the motion of the capsule evolves per some variation of the Navier-Stokes equations. This paper uses the hydrodynamic code Freyja, a 1D Lagrangian model using a single fluid approximation with two temperatures, one for electrons and one for ions.

Freyja also contains several other physics packages which govern how laser energy is coupled to the target and how that energy is transported through the target, more details of these models are given in Sec. II B. No model is genuinely perfect and often requires approximations and control parameters to tune it to match what is seen in the physical world. This is particularly true for ICF simulations in which several parameters must be set to control a variety of physical behaviours. Such examples include the amount of laser energy expected to couple to the target, the amount of free-streaming ion/electron flux, the fraction of laser energy lost due to laser-plasma instabilities (LPIs) and the fraction of absorbed energy at the critical surface via resonance absorption. These parameters can sometimes be interpreted from physical intuition but are often tuned to match pre-

vious experimental work.

In this paper, Gaussian process (GP) regression techniques are used to generate a surrogate model trained from a variety of Freyja simulations (≈ 100), with changing values of laser coupling fraction (C), LPI loss fraction (LPI), resonant absorption fraction (RA) and flux limiter for both ions and electrons ($f_i,\ f_e$). The surrogate is then used to predict what values of input parameters result in best matching to experimental results given in Goncharov *et al.* [1]. The experimental results given in Goncharov *et al.* are for the observed shock velocity through a CH foil driven by a variety of laser pulse designs which mimic the the early stage of implosion in direct-drive ICF.

The next section of this paper (Sec. II will discuss in more detail how Freyja simulates laser-driven implosion and how thermal transport is modelled. In Sec. III, further details on how the simulations are set up and how the GP surrogate is trained and used are described. The final two sections (Sec.IV & V) discuss the found results and conclude on what is found and could be improved.

II. THEORY

A. Hydrodynamic Modelling

The CH foil is modelled as a mesh of fluid elements storing the initial values of density ρ and specific internal energy ϵ. For a Lagrangian model, the boundaries of the mesh grid moves with the fluid velocity u. The hydrodynamic package in Freyja aims to solve the Euler equations:

$$\frac{D\rho}{Dt} + \rho\nabla\cdot\mathbf{u} = 0; \tag{1}$$

$$\rho\frac{D\mathbf{u}}{Dt} + \nabla P = 0; \tag{2}$$

$$\rho\frac{D\epsilon}{Dt} + P\nabla\cdot\mathbf{u} = 0. \tag{3}$$

where, P is the pressure and the differential operator for 1D planar geometry is $\frac{D}{Dt} = \frac{\partial}{\partial t} + u\frac{\partial}{\partial x}$. The fluid properties stored in each grid element are then calculated by the spatial derivatives of the Euler relations, evolving the grid for the next time step. The equations need to be closed, requiring a relation between P and ϵ. In Freyja the equation of state (EOS) used is for an ideal gas, $P = (\gamma - 1)\,\rho\epsilon$ where γ is the adiabatic index. The evolution of the grid is split into a solver for the Euler equations and thermal transport, given in more detail in Sec.II B. As the mesh moves with the fluid, the matter is not transported between computational cells, making a Lagrangian more straightforward and advantageous when concerned about numerical mixing [3]. The momentum conservation law displayed in Eqn. 2 in planar in geometry is often referred to as the inviscid Burgers' equation which governs the evolution of acoustic waves, therefore including expansion and shock waves. Given the adiabatic nature of the Euler equations, no entropy waves and thus no contact discontinuities are described by such equations. Therefore an extra dissipative model known as artificial viscosity [4] is required to capture the effects of an increase in entropy due to shocks. The artificial viscosity modifies the Euler equations such that $P \to P+Q$, where Q is the additional pressure. The model used in Freyja is the Kuropatenko form of Q outlined in [5],

$$Q_{Kur} = \rho\frac{c_2\,(\gamma+1)}{4}\,|\Delta\mathbf{u}|^2 + \sqrt{\rho^2 c_2^2\left(\frac{\gamma+1}{4}\right)^2(\Delta\mathbf{u})^4 + \rho^2 c_1^2 c_s^2 \Delta\mathbf{u}^2}. \tag{4}$$

where $c_{1,2}$ are constants often set to unity and c_s is the speed of sound. This provides the required dissapative model without producing large nonphysical oscillations. To restrict the shocks to specific grid cells, a flux limiter is used to restrict where artificial viscosity is used. Therefore the value of Q between the i^{th} and j^{th} cell is $Q_{ij} = Q_{ij,Kur}\,(1-\psi_{ij})$, where the form of the flux limiter ψ_{ij} is described by Caramana et al. [5].

B. Energy Transport Model

1. Laser Deposition Model - Inverse Bremsstrahlung

The simple classical process for the interaction between laser light and matter is described by inverse bremsstrahlung (IB). Consider an electron experiencing an electric field of that of a plane wave, the equation of motion is given for this electron to be

$$\frac{\mathrm{d}\boldsymbol{u_e}}{\mathrm{d}t} + \nu_{ei}\boldsymbol{u_e} = \frac{q_e\boldsymbol{E}}{m_e}, \tag{5}$$

where the approximate drag ($\nu_{ei}\boldsymbol{u_e}$) on the electrons is due to electron-ion collisions at a rate of ν_{ei} per second [6]. The dispersion relation from this simple model encapsulates the physics for IB. Assuming the electron plasma frequency is much higher then the frequency of the electron-ion collisons ($\nu_{ei} << \omega_{pe}$), the dispersion relation derived in [7] states:

$$k \approx \pm\frac{\omega_L}{c}\left(1 - \frac{\omega_{pe}^2}{\omega_L^2}\right)^{\frac{1}{2}} f(\omega_L), \tag{6}$$

$$f(\omega_L) = \left[1 + i\frac{\nu_{ei}}{2\omega_L}\frac{\omega_{pe}^2}{\omega_L^2}\frac{1}{1-\omega_{pe}^2/\omega_L^2}\right], \tag{7}$$

where $\omega_{pe} = \sqrt{n_e e^2/\epsilon_0 m_e}$ and ω_L is the laser driver angular frequency. The value of k is observed to be

driven to zero when $\omega_L = \omega_{pe}$, therefore the laser can no longer couple to the plasma beyond this critical surface defined by the critical surface density n_c. The presence of an imaginary term shows that the laser light experiences damping when propagating through the ablator. This can be described by the absorption coefficient $\kappa_{ib} = 2\mathrm{Im}\,(k)$, since intensity $\propto |\boldsymbol{E}|^2$. Using the expression for ν_{ei} in [8], κ_{ib} is found to be:

$$\kappa_{ib} = \frac{e^6}{3\epsilon_0^3 c\,(2\pi m_e k_B)^{3/2}} \frac{Z^2 n_i n_e \Lambda_{ei}}{T_e^3 \omega_0^2 \epsilon_0}, \tag{8}$$

where Z is the atomic number of the plasma, n_e,n_i are the electron and ion number density, T_e is the electron temperature, Λ_{ei} is the (electron-ion) Coulomb logarithm and $\omega_0^2 = \omega_{pe}^2 + c^2k^2$. The absorption coefficient can be reformulated such that $\kappa_{ib} \propto (1 - n_e/n_c)^{-1/2}$, which reflects the fact that a large fraction of IB absorption occurs near the critical surface.

The energy loss due to IB is calculated in Freyja using

$$\frac{dE(t)}{dx} = -\kappa_{ib} E. \tag{9}$$

Here $E(t)$ is the time-dependent energy of the laser initialised at each time step to be $E = \Delta t P$, where P is the laser power profile specified for the implosion. There are several other processes which affect the amount of laser energy that is transferred to the CH plasma. Three such processes considered in Freyja are controlled via input parameters.

2. *Laser Deposition Model - Laser Coupling*

In reality, not all incoming laser energy will be transferred to the target/plasma. In Freyja, the fraction of energy transferred to the plasma is controlled via a user input variable with a value between zero and one, zero being no energy being transferred, and one being all of the energy being transferred. This input variable is used as a proxy for physical processes such as cross-beam energy transfer, which reduces the laser energy transferred to the target. The coupling parameter C is chosen to be within the range $0.65 \leq C \leq 0.95$, which gives an ideal range in which enough energy should couple to the target to simulate shocks.

3. *Laser Deposition Model - Resonant Absorption*

Plasma produced by the interaction of the laser with a solid target creates an inhomogeneous density ramp, which comprises a under- ($n_e < n_c$) and over-dense ($n_e > n_c$) regions. When laser light interacts with such a density profile, electrostatic waves are excited if any electric field component matches the direction of the density gradient (known as p-polarised interaction). Close to the boundary of the two regions ($n_e \approx n_c$), the magnitude of the electric field component becomes very large, and waves are resonantly excited. In this plasma region, energy is transferred from the EM wave into plasma waves, which eventually is converted into thermal energy as these waves are damped via collisions or Landau damping. Previous work done by Ginzburg (1961) and Pert (1978), discussed in Pfalzner ([8]), estimates that for a linear density profile, up to 50% of absorption can occur through this process. This estimation defines a suitable range of values that the resonant absorption fraction should take in Freyja. In this paper, the resonant absorption fraction RA, is taken to be within the range, $0.15 \leq RA \leq 0.45$.

4. *Laser Deposition Model - Laser-Plasma Instabilities*

Laser-plasma instabilities in the coronal plasma region also play a significant role in ICF experiments. Often these are three-wave parametric instabilities, where the incident (laser) wave resonantly decays into two new waves. These new waves can be either scattered electromagnetic waves or plasma (electron or ion) waves, depending on the frequency of the laser light and the density region of the plasma. The presence of such instabilities also hinges on the incoming laser intensity, such that if the incoming intensity is below the instability threshold, the instability should not occur. The laser profiles used in this paper are taken from Goncharov et al. [1]. With the intensity magnitudes used in these designs, it is assumed that stimulated Raman scattering will be the dominant instability. The energy loss due to LPI's will be extracted at the quarter critical density ($n_e = n_c/4$) to represent this. Freyja has an additional parameter that acts as a proxy for energy loss due to LPI generation, where the fraction of laser energy lost due to these processes can be set. The exact details and modelling of LPIs cannot be done at hydrodynamic time scales, so until a suitable surrogate model can be built, such a parameter is useful. The LPI loss fraction was taken to vary within the range of 5% to 35% energy loss i.e $0.05 \leq LPI \leq 0.35$.

5. *Thermal Conduction*

The transport of the energy coupled to the plasma near this critical surface is then transported to the ablation surface via thermal conduction. To first order one can treat the process as electrons diffusing through a background of fixed ions. In Freyja this done using the Braginskii thermal conduction model [9]. Braginskii stated the parallel heat flux ($q_{i,e} = -\kappa_{i,e}\nabla T_{i,e}$) for electrons and ions to be

$$q_e = -\frac{\kappa_0 \gamma\,(Z)\, T^{5/2}}{Z\Lambda_{ie}} \nabla T_e \tag{10}$$

$$q_i = -3.906 \left(\frac{2m_e}{m_i}\right)^{1/2} \frac{\kappa_0 T^{5/2}}{Z^4 \Lambda_{ii}} \nabla T_i \tag{11}$$

where

$$\kappa_0 = \frac{12\pi^{3/2}\epsilon_0^2 k_B^{7/2}}{\sqrt{2m_e}e^4}. \tag{12}$$

The function $\gamma(Z)$ is tabulated in [9], however Freyja uses the approximation by Manheimer [10]

$$\gamma(Z) = 13.6\frac{Z+0.24}{Z+4.24}. \tag{13}$$

Due to the dependency on mass shown in eqn 11, the thermal conduction process is dominated by the much lighter and faster electrons.

The thermal transport is then modelled in Freyja by solving the non-linear conduction equation built upon the Braginskii conductivity $\kappa_{i,e}$,

$$c_V \frac{\partial T_{i,e}}{\partial t} = \nabla \cdot (\kappa_{i,e} \nabla T_{i,e}). \tag{14}$$

Non-local effects caused in areas where the mean free path becomes significantly larger than the physical length scale (defined as areas of large Knudsen numbers), result in the reduction of the classical heat flux model defined by Braginskii. This is modelled using the Larsen flux limiter which alters κ to restrict the amount of free-streaming flux $f_{fs} = v_{th} n k_B T$ with thermal velocity $v_{th} = \sqrt{2k_B T/m}$. The formulation for the modified conductivity ($\kappa^{'}$)is taken from the work of Olson [11] with

$$\kappa^{'} = \left(\frac{1}{\kappa^2} + \left(\frac{1}{f_0 f_s}|\nabla T|\right)^2\right)^{-1/2}. \tag{15}$$

Typical values for electron flux limiters are within the range $0.04 \leq f_e \leq 0.1$ [1], as these values tend to best match experimental results. Less was known about the range of values for the ion flux limiter, so the parameter space was chosen to be around the Freyja default value of 0.5, such that $0.35 \leq f_i \leq 0.65$. The electron flux was chosen to vary between $0.0 \leq f_e \leq 0.3$ to match the domain sizing for the other parameters.

III. SIMULATION SETUP METHODOLOGY

1. *Freyja Set-up*

The setup for Freyja is chosen such that it matches the experimental design discussed in Goncharov et al., where a shock is tracked through a CH foil with a thickness of 125 μm. This 125-micron region is simulated in Freyja and split into 2000 grid cells with an initial density of 1050 kgm^{-3}, and the total time evolution of the foil is simulated for 6.0 ns. As alluded to earlier, the laser profiles used are also taken to be those used in [1] and are shown in Fig.2.

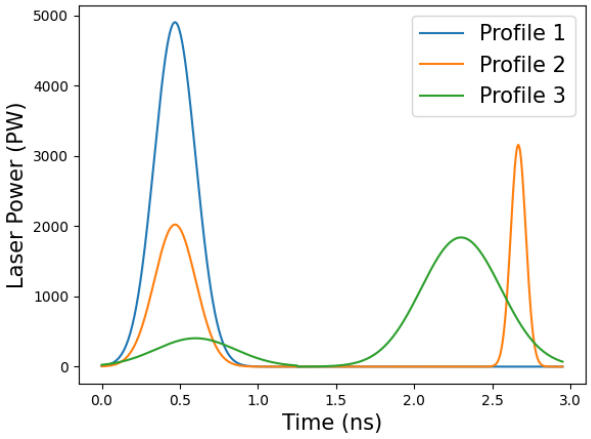

FIG. 2: Laser profiles used to in Freyja to re-create experimental results in Gonchorov et al. [1]

The shock velocity data needed to be extracted to compare the experimental results and simulations in Freyja. The WebPlotDigitizer software (https://automeris.io/WebPlotDigitizer/) extracted data points within the range given in Figs 3a, 3b and 4 shown in the paper. Gaussian process regression was used to find a mean experimental result profile and confidence limit to try and match the Freyja simulations. Specifically, the metric used to judge how close the simulation result matched the experimental data was the log of the likelihood distribution which was assumed to be Gaussian ($\log \mathrm{P}\left(\mathbf{U_{Exp}}|\mathbf{t}, \theta, \sigma_{Exp}\right)$), such that:

$$\log \mathrm{P} = -\frac{1}{2\sigma_{Exp}^2} \sum_{i=1}^{N} \left(U_{Exp,i} - f(\mathbf{t_i}, \theta)\right)^2 - C \tag{16}$$

where N is the number of data points, σ_{Exp} is the standard deviation found from the Gaussian regression using an exponential kernel on the experimental data sets, C is a constant given as $N \log \sigma_{Exp} - \frac{N}{2} \log 2\pi$, and $U_{Exp,i}$ and $f(\mathbf{t_i}, \theta)$ are the experimental and simulation shock velocity results.

The shock velocity is estimated by tracking the location of the shock front at each time step, recording both the position and time at each iteration. As the laser is incoming from the right-hand boundary, the shock front moves from right to left, with the shock front being observed as a discontinuity in the density profile. The density profile was searched from left to right (i.e. in the opposite direction to the travelling shock) to find the first data point, which had changed by about 5% of the original CH density. This represented the last point untouched by the shock, thus estimating the position of the shock front. Visualisation of this method is shown in Fig.3. The tracking was done at set regular intervals (i.e. every ten outputs) rather than every output to remove nonphysical oscillations in the data to get a smoother velocity profile.

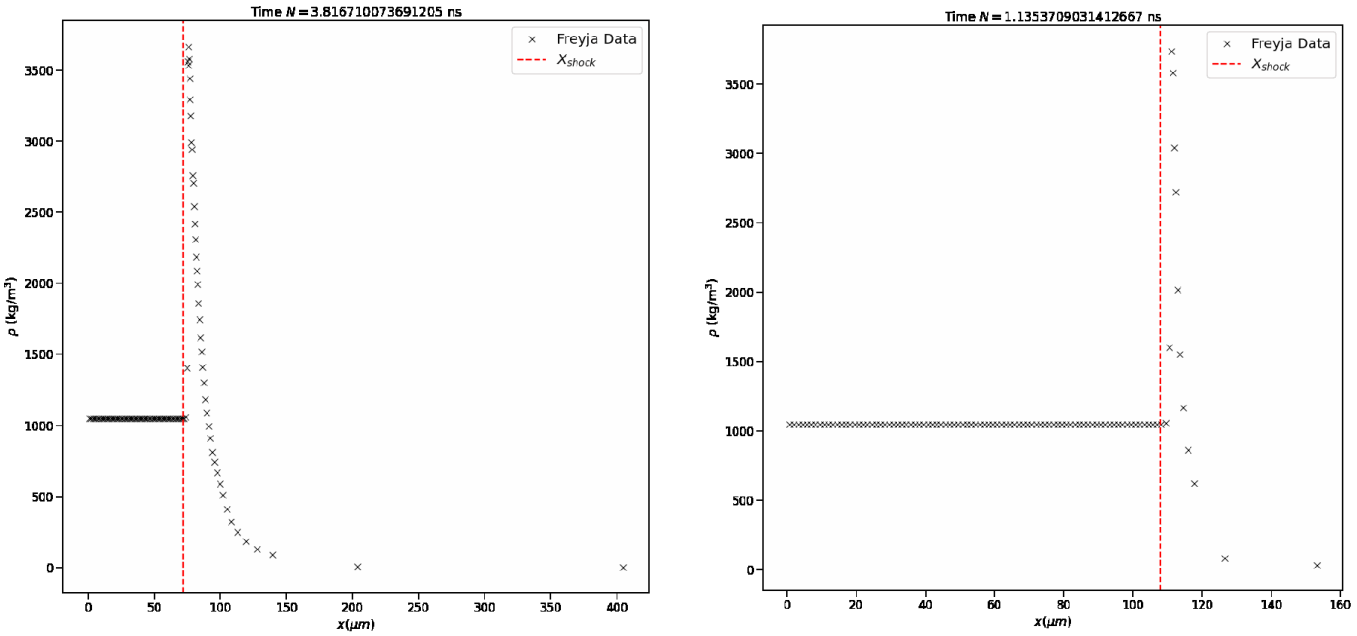

FIG. 3: Visualisation of the shock front (red dashed line) tracking, using the density profile over the simulation grid space (black crosses).

From the definition of the log-likelihood given by Eqn.16, the length size of the experimental data set and simulation result need to be equal and compared over the same time interval. A further Gaussian regression fit was performed on the simulation data set, again using an exponential kernel to ensure this was done. The fit estimates the shock velocity result of Freyja across the experimental time interval and interpolates the missing time data values to match the size of the two data sets.

2. *Building GP Surrogate*

One hundred Latin-hypercube (LH) samples were produced for the five variable parameter space (θ) to train a GP surrogate, where:

$$\theta \in \{[f_e, f_i, RA, C, LPI]\}, \tag{17}$$

for which the space from which was sampled is defined using the bounds discussed in the previous section. These LH samples set the input parameter values for Freyja simulations, in which the recorded log-likelihood is recorded and stored as part of the output training set. These input and output sets are then used to train a GP surrogate using an exponential kernel to make predictions for a larger LH sample space, which was chosen to be 50,000 samples. This enabled many estimations for the log-likelihood to be found without performing long simulations to be more efficient with time. The best fit is then found to be for the LH sample that predicts the highest (lowest negative) value of the log-likelihood, and these input parameters should then be found to match Freyja simulations to the experimental data.

Sensitivity to the input parameter values is also discussed, where the first-order sensitivity is estimated using the kernel length scales for each parameter. The inverse of these length scales estimates this first-order sensitivity. However, to make more meaningful comparisons between the parameters, the inverse length scales are multiplied by the average value of each parameter judged from the Latin hypercube samples.

IV. RESULTS AND DISCUSSION

A. Profile 1 Surrogate

The first profile a surrogate was created for was the single picket laser profile labelled as profile 1 in Fig. 2. The Gaussian surrogate model predicted the optimal input parameters (i.e leads to the minimal log-likelihood), to be $\theta = [0.2715, 0.6275, 0.393, 0.6737, 0.3185]$. The surrogate prediction matches the experimental results across the whole experimental domain and the breakout time, where the shock exits the foil and the velocity falls to zero.

In Goncharov et al., they perform LILAC simulations using this laser and target system for an electron flux limiter of 0.04, 0.06 and 0.1. These simulations found that a flux limiter value of 0.06 accurately matched these results, significantly smaller than the value predicted from the Gaussian surrogate. However, the Gaussian surrogate is not solely dependent on f_e. The simulations per-

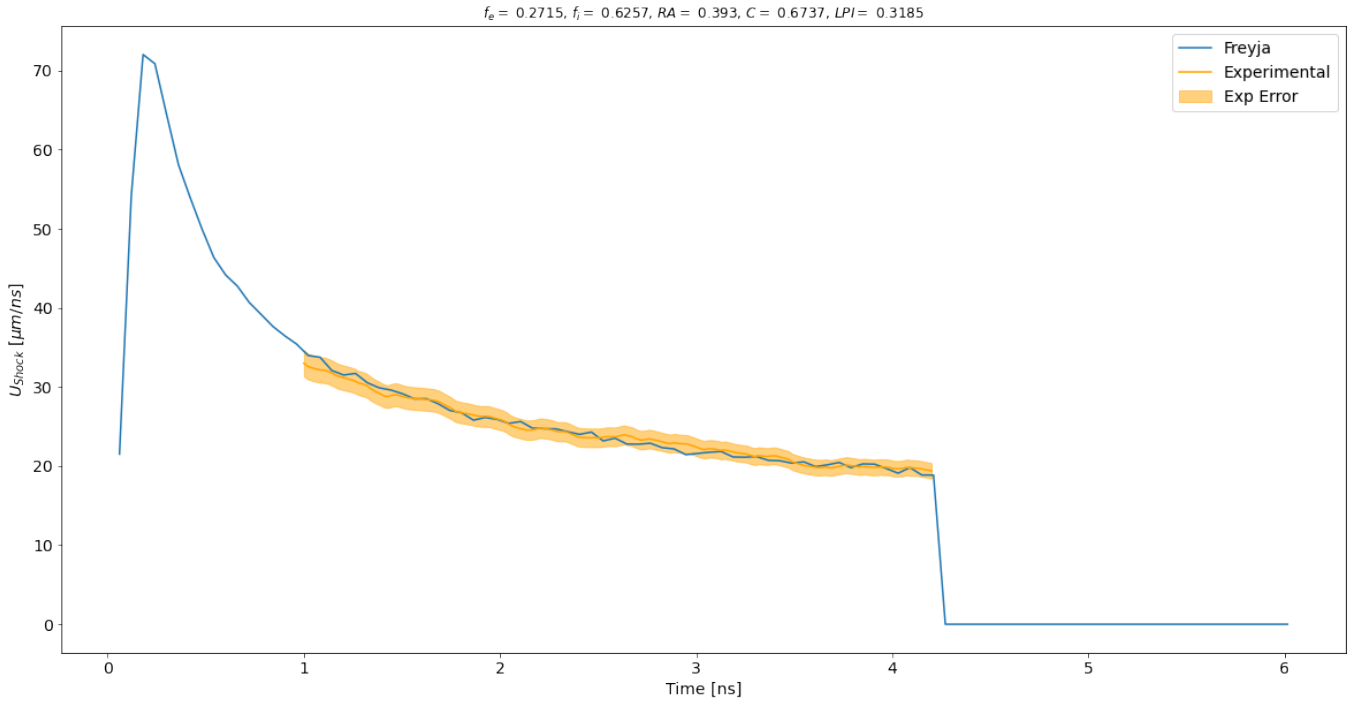

FIG. 4: Surrogate model prediction for the single picket design (profile 1). The Freya output is observed to match the experimental result closely and manages to match the breakout time almost exactly with input parameters equal to $\theta = [0.2715, 0.6275, 0.393, 0.6737, 0.3185]$. However, the surrogate estimates the value of f_e to be significantly larger than those simulated by LILAC simulations shown in Goncharov et al. [1].

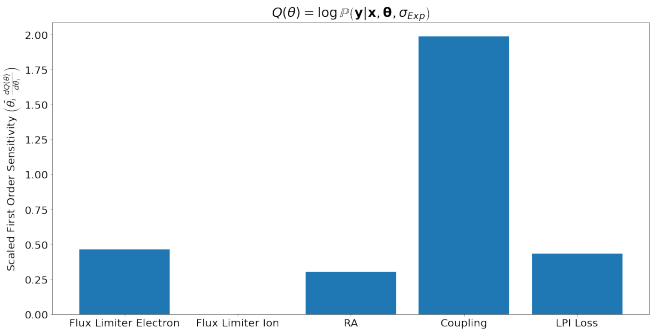

(a) Sensitivity analysis of the input parameters for the profile 1 Gaussian process surrogate.

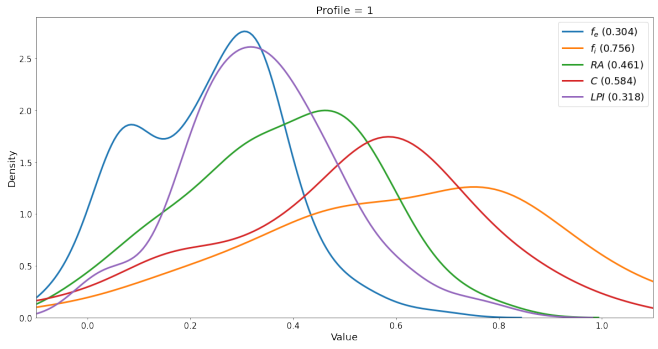

(b) Posterior distributions of parameters using the Gaussian surrogate data. These distributions were estimated using Markov-Chain-Monte-Carlo methods.

FIG. 5: Sensitivity analysis (left) and resulting posterior distribution of parameters from MCMC (right).

formed in Goncharov et al. only looked at altering the value of f_e, and our result may suggest that the flux limiter may not be the most sensitive parameter in this case.

Sensitivity analysis was performed using the estimated kernel length scales for each parameter (i.e. the inverse of this scale) to observe whether the electron flux limiter is the most sensitive parameter or not.

The resulting sensitivity analysis shown in Fig.5a shows that it is the laser coupling that is the dominant parameter when trying to match Freyja to the experimental result. This makes sense if we consider that without enough laser energy being coupled to the surface, there would be little thermal energy to transport which renders the flux limiter terms to be mute if this is true. The strength of shocks and, therefore, their speed depends on how much laser energy can be transferred to the material, so observing the coupling sensitivity to be maximal is expected. All other sensitivities are roughly equal, except for the ion flux limiter, which is observed to have little to no impact on the result for the range of values it has been sampled.

However, considering how heavy the ions are relative

to the electrons within the plasma, we would expect electron thermal conduction to dominate by a rough factor of $m_i/m_e \approx 1836$, resulting in sensitivity in f_i is to be expected.

The sensitivity analysis results help explain why a higher value of f_e is observed, with the resulting prediction being more favourable to matching the correct coupling over the electron flux limiter. However, it still leaves some questions over what range of values is optimal for these parameters for modelling this experiment.

Markov-Chain Monte-Carlo (MCMC) methods were used to estimate each parameter's posterior distributions using the Metropolis-Hastings algorithm with a Gaussian distribution form for the transition probability (Gaussian random walk). The prior distribution for the chosen parameters was taken to be a multivariate Gaussian, with the means chosen to be the resulting values predicted from the GP surrogate (Fig.4).

The resulting distributions given in Fig.5b, show the distributions peak at values close to that of the GP surrogate result, shown in Fig.4. Interestingly, the f_i distribution is observed to have less of a bell-shaped curve and tends more towards a flat nature, perhaps due to its very low sensitivity and, therefore, little impact on the simulation result.

A secondary peak is observed in the f_e distribution, close to the range of values from which we expected f_e to initially be from the Goncharov et al. results (0.04 - 0.1). This suggests that other results match the experimental results within this area, which were not picked up due to their slightly larger log-likelihood result.

B. Profile 2 Surrogate

The second profile which was looked at was a double picket Gaussian pulse design shown by the orange curve in Fig.2. The FWHM of the pickets is the same as that of the first profile. However, we now consider a system where two smaller shocks are generated, which coalesce within the CH foil. This is closer to what is commonly used in ICF experiments.

The Gaussian surrogate model is once again shown to nicely predict a set of Freyja input parameters which match closely to the experimental results of Goncharov et al., with the parameter set predicted to match the experimental data found to be optimal, $\theta = [0.0530, 0.4571, 0.307, 0.7573, 0.1542]$. The predicted result matches the experimental estimate almost identically up to 2.5 ns. After this point, the experimental profile predicts a plateau velocity profile, with the Freyja result taking more of an exponential tail trend. This is likely due to an error in how the experimental profile is estimated from Goncharov et al. and is not a cause for concern. The prediction is observed to accurately match the shock coalescence time at around 3.5 ns, which is one of the more critical features to match, as many ICF experiments depend on estimating when respective shocks will coalesce.

The prediction beyond the shock matching time is again observed almost identically to match the experimental profile. However, disappointingly, the prediction estimates a breakout time which is around 0.2 ns larger than that found in Goncharov et al..

In contrast to the previous result, the predicted value of f_e is relatively close to the 0.06 value predicted by Goncharov, and significantly more laser energy needed to be coupled to the CH foil than for the previous experiment.

Once again, performing sensitivity analysis on the surrogate model, we find that the laser coupling parameter is the most dominant source of sensitivity to the predicted log-likelihood. The other parameters have a similar magnitude of sensitivity as observed in the profile 1 surrogate. However, the sensitivity of the coupling parameter is now doubled. This is likely since we are now simulating two shocks which must be matched at the correct time. Thus, the amount of energy required to be coupled to the surface is even more important, for the strength of the shocks needs to be perfectly tailored.

Posterior distributions found from MCMC methods show that the value of f_e is most likely to be around 0.06, which was expected from the literature, with a sharp peak at this value. The other parameters have more of a spread. Once again, the ion flux limiter distribution shows more of a flat nature than a bell-shaped curve observed in other parameter distribution curves.

C. Profile 3 Surrogate

The final laser profile, which is considered, is once again a double pulse design. However, this profile uses larger width pulses and reduced peak power. The surrogate prediction for this profile ($\theta = [0.0315, 0.3624, 0.1820, 0.9467, 0.0572]$) closely matches the shock time and the velocity trend, but it fails to match the experimental result pre-shock coalescence. The Freyja profile shown in blue in Fig.8 is observed to always be below the 95 % confidence range for the experimental data set at this stage. However, it does appear to have a similar gradient during this period.

The experimental data set for this profile was very sparse (Figure 4. in [1]), with the majority of the experimental result having to be estimated using a mix of this data set and the LILAC simulations performed in Goncharov et al.. Therefore, the surrogate prediction and experimental result discrepancy are likely due to this sparsity in experimental data. The other two surrogates could match their respective profiles to a higher degree of accuracy. Another issue arising from the sparse experimental data is that the experimentally predicted breakout time is less obvious, so any comparisons between the surrogate predicted breakout time and experimentally predicted breakout time cannot be made. Even though this profile was more difficult to make accurate predictions with, it still showed that this simple GP sur-

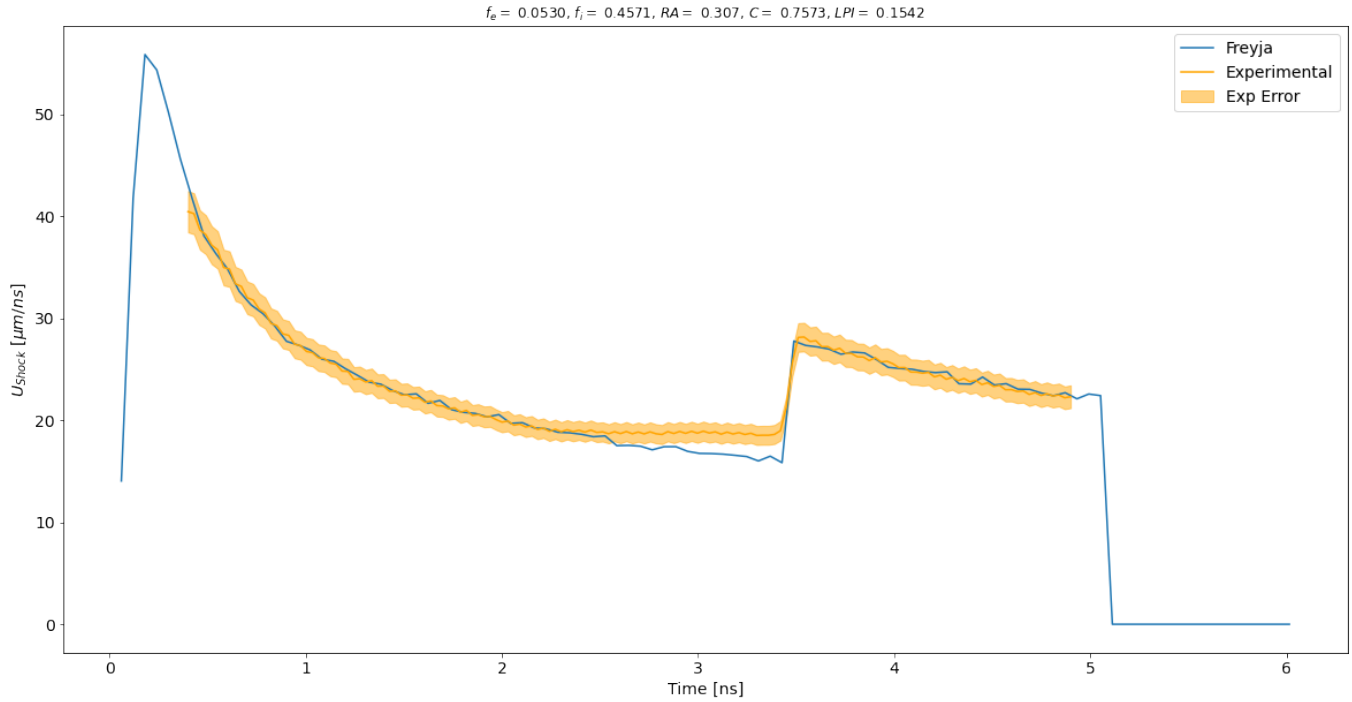

FIG. 6: Surrogate model prediction for the first double-pulse laser profile (profile 2). The prediction matches the experimental data pretty well, except for the slight deviation around 2.5 ns, where the experimental profile appears to plateau rather than an exponential tail. The shock coalescence time is matched well as the two discontinuity lines overlap. However, the breakout time is off by about 0.2 ns. The input parameters that were predicted by the GP was $\theta = [0.0530, 0.4571, 0.307, 0.7573, 0.1542]$.

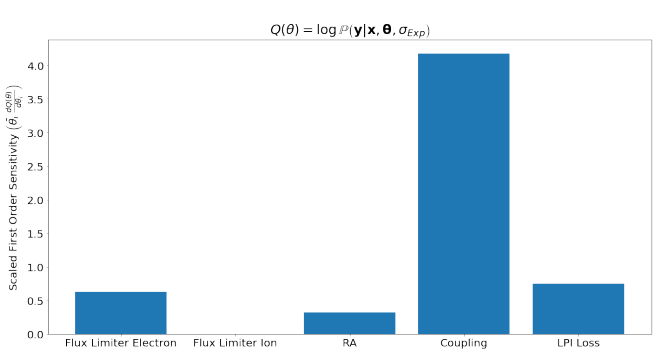

(a) Sensitivity analysis of the input parameters for the profile 2 Gaussian process surrogate.

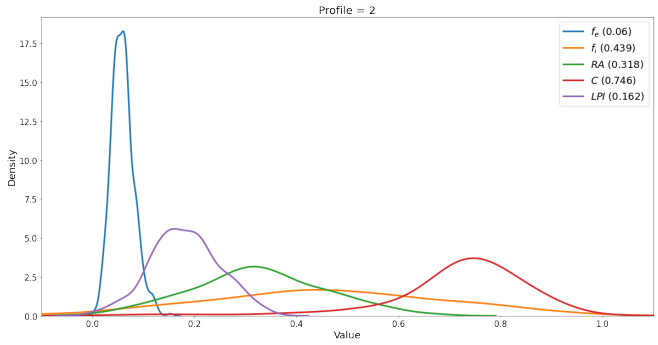

(b) Posterior distributions of parameters using the Gaussian surrogate data. These distributions were estimated using Markov-Chain-Monte-Carlo methods.

FIG. 7: Sensitivity analysis (left) and resulting posterior distribution of parameters from MCMC (right).

rogate method could match fairly close to observed experimental results and help determine what values for specific input parameters are best to use without needing to run large amounts of hydrodynamic simulations. Looking at the sensitivity analysis results (Fig.7a), we can once again see that the laser coupling parameter is the most sensitive. However, the electron flux limiter appears to be more important for this model than the other profile surrogates. Interestingly, we can see that the coupling is observed to be much higher for this profile than in the previous two setups, with almost all the laser energy needing to be coupled to the surface ($\approx 95\%$). This could be due to the alternative nature of this profile compared to the previous designs. We irradiate the foil over a longer period and thus apply a larger amount of laser energy over the entire 3.0 ns period than the other profiles. The surrogate prediction also predicts a far lower fraction of energy going into $LPI's$ than the other two profiles, which is encouraging, as this laser profile uses lower intensity laser pulses. Given that the presence of

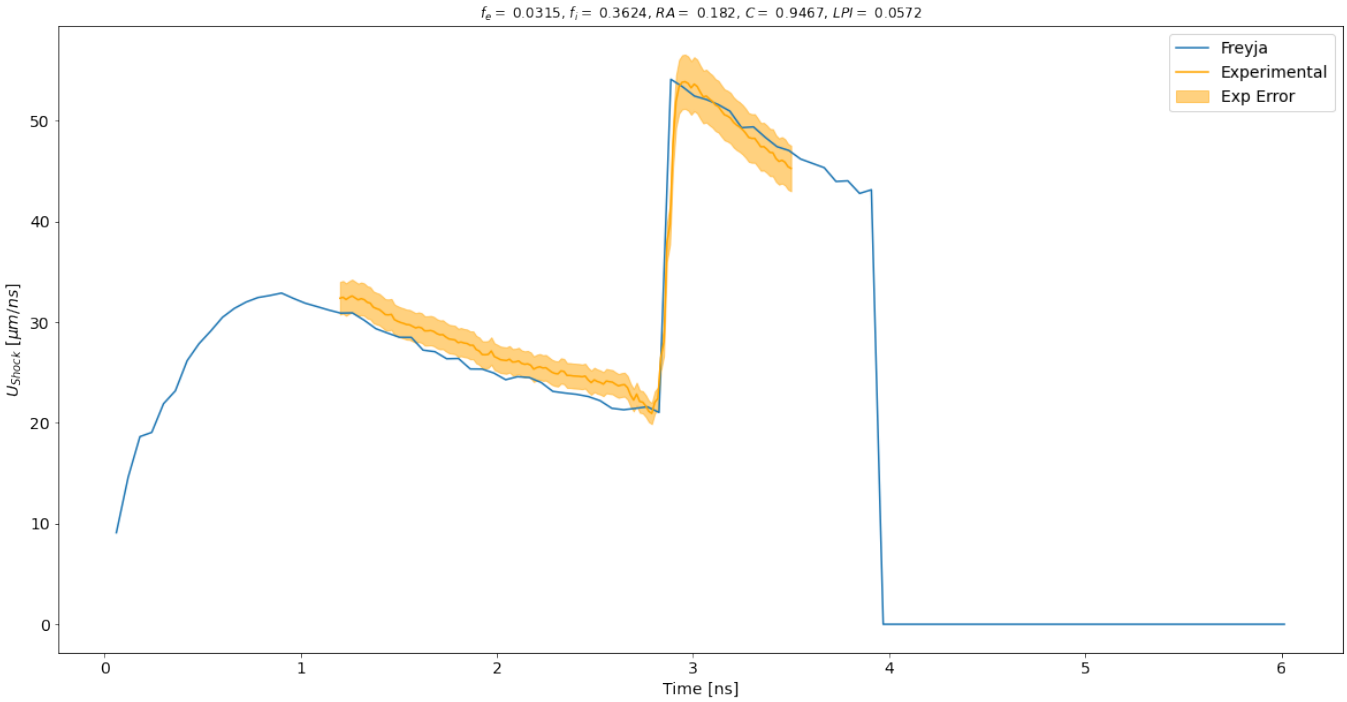

FIG. 8: Surrogate model prediction for the alternative double-pulse laser profile (profile 3). The prediction matches the experimental data closely at the shock time and after the coalescence. However, before the second shock, it fails to be within the 95% confident limit. The experimental data set for this was sparse in this region, suggesting more information is needed to make a more accurate prediction. The input parameters that were predicted by the GP was $\theta = [0.0315, 0.3624, 0.1820, 0.9467, 0.0572]$.

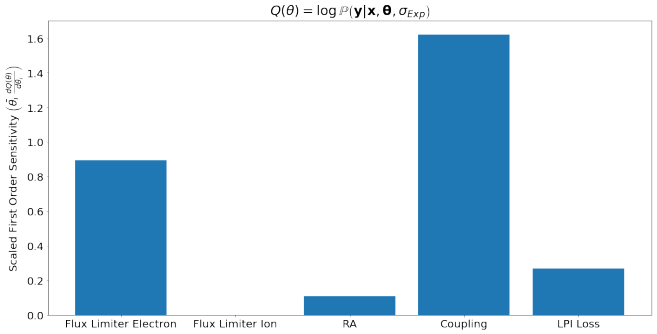

(a) Sensitivity analysis of the input parameters for the profile 3 Gaussian process surrogate.

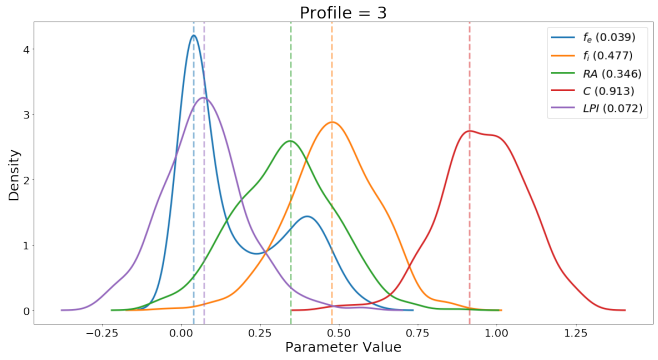

(b) Posterior distributions of parameters using the Gaussian surrogate data. These distributions were estimated using Markov-Chain-Monte-Marlo methods.

FIG. 9: Sensitivity analysis (left) and resulting posterior distribution of parameters from MCMC (right).

LPI's is more likely as laser intensity increases, this result is promising as it shows that the surrogate model technique does not predict something nonphysical.

Once again, MCMC methods were used to estimate the posterior distributions for each of the parameters (Fig.9b). All the distributions are observed to peak close to the prediction shown in Fig.8.

V. CONCLUSION

Gaussian process regression techniques were used to generate surrogate models which estimated the value of specific input parameters such as laser coupling, LPI loss, resonant absorption fraction and electron/ion flux limiters. The resulting surrogates were observed to find sets of input parameters that closely match the experimental results discussed in Goncharov et al. [1] for shock veloc-

ity data through a CH foil. The predicted magnitude of f_e was found to deviate from the LILAC simulations displayed in Goncharov et al. in some cases. However, from performed sensitivity analysis, it was observed that the laser coupling parameter was the most sensitive parameter, which was not altered in the LILAC simulations.

The surrogate predictions were shown to accurately match the shock timing for multiple picket laser profiles. However, the surrogate would not be able always to match the breakout time observed in the experimental data. This would suggest that further improvements to the surrogate model are required to incorporate accurate matching of the shock and breakout timings. One way to do this could be to solely focus on designing metrics which aim to compare how the shock and breakout times of Freyja simulations match the experimental result rather than the entire velocity profile to train the GP surrogate. The surrogate model discussed in this paper could easily be altered to incorporate this by using the log-likelihood of the breakout and shock times rather than the log-likelihood of the entire profile to train the GP surrogate. If the shock and breakout times match, the rest of the velocity profile should also then match the experimental result.

To conclude, the GP surrogate models discussed in the paper were able to help infer what values of input parameters would be best to use for particularly laser profile designs and allowed for this to be done more efficiently, as tens of thousands of predictions could be made in seconds, which would take significantly longer if this was done performing tens of thousands of Freyja simulations.

[1] V. Goncharov et al, Early stage of implosion in inertial confinement fusion: Shock timing and perturbation evolution, Phys. Plasmas **13**, 012702 (2006).

[2] R. Craxton et al, Direct-drive inertial confinement fusion: A review, Phys. Plasmas **22**, 110501 (2015).

[3] C. Laney, *Computational Gasdynamics* (Cambridge University Press, 1998).

[4] M. Wilkins, Use of artificial viscosity in multidimensional fluid dynamic calculations, Journal of Computational Physics **36**, 281 (1980).

[5] S. M. Caramana, E.J. and P. Whalen, Formulations of artificial viscosity for multi-dimensional shock wave computations, Journal of Computational Physics **144**, 70 (1998).

[6] E. Morse, *Nuclear Fusion* (Springer, 2019).

[7] E. Morse, *Physics of laser fusion. Vol. I. Theory of the coronal plasma in laser-fusion targets* (1981).

[8] S. Pflazner, *An Introduction to Inertial Confinement Fusion* (CRC Press, 2006).

[9] S. Braginskii, Transport processes in a plasma, Reviews of plasma physics **1**, 70 (1965).

[10] C. D. Manheimer, W. and V. Goncharov, The development of a krook model for nonlocal transport in laser-produced plasmas. i. basic theory, Phys. Plasmas **15**, 083103 (2008).

[11] A. L. Olson, G.L and M. Hall, Diffusion, p_1, and other approximate forms of radiation transport, Phys. Plasmas **64**, 619 (2000).